



Integrated calcareous nannofossil and stable isotope stratigraphy across the Danian-Selandian boundary, west central Sinai, Egypt

MAHMOUD FARIS, SHERIF FAROUK, SREEPAT JAIN, FAYEZ AHMAD, GAMAL MUSA, MOHAMED SHAMA AND FATMA SHAKER

LETHAIA



The stratigraphical range of bioevents across the Danian-Selandian (D/S) boundary are analysed using calcareous nannofossils and stable isotopes ($\delta^{13}\text{C}$ and $\delta^{18}\text{O}$) from the Ekma section, west central Sinai (Egypt). Three calcareous nannofossil zones are recorded (from bottom to top): NP3, NP4, and NP5. Based on this, the Ekma section is the first nearly complete section from Egypt, straddling the D/S boundary. The D/S boundary is placed at the Lowest Occurrence (LO) of *Lithoptychius ulii* (base NTP8B). The LOs of *L. varolii*, *L. pileatus*, *L. schmatzii*, and *Fasciculithus involutus* are delayed, either as a result of diachronous and/or environmentally-controlled conditions. Two negative $\delta^{13}\text{C}$ excursions are recorded that are associated with falling sea levels. The first one (CIE-DS1) is observed through the latest Danian Event (LDE) and within the calcareous nannofossil subzones NTP7B and NTP8A, whereas the second one (CIE-DS2) occurs within the NP5 Zone (at the top of the Dakhla Formation). No significant changes are noted in the calcareous nannofossil species distribution patterns over the D/S boundary. However, there is a distinct change in the trophic structure and water-mass properties, i.e., from cool and mesotrophic (coincident with a decrease in the relative sea-level) to warm and oligotrophic conditions. There is also a gradual increase in both species diversity and warm and oligotrophic conditions with a corresponding drop in species dominance throughout the three studied intervals, pre-LDE, LDE and post-LDE. □ *Calcareous nannofossil, stable isotope, Danian, Selandian, Sinai, Egypt*

Mahmoud Faris [mhmfaris@yahoo.com], Gamal Musa [dr.deo.sherif@gmail.com] & Mohamed Shama [mohamedshama400@gmail.com], Department of Geology, Faculty of Science, Tanta University, Tanta, Egypt; Sherif Farouk [geo.sherif@hotmail.com], Exploration Department, Egyptian Petroleum Research Institute, Nasr City, Egypt; Sreepat Jain [sreepatjain@gmail.com], Adama Science and Technology University, Department of Applied Geology, School of Applied Natural Sciences, Adama, Ethiopia; F. Ahmad [fayeza@hu.edu.jo], Department of Earth and Environmental Sciences, Prince El-Hassan Bin Talal Faculty for Natural Resources and Environment, The Hashemite University, Zarqa, Jordan; Fatma Shaker [felkammam@gmail.com], Department of Geology, Faculty of Science, Benha University, Egypt & Department of Geological Engineering, Faculty of Mines, Istanbul Technical University, Istanbul, Turkey; manuscript received on 21/02/2024; manuscript accepted on 12/08/2024; manuscript published on 06/12/2024 in *Lethaia* 57(4).

Globally and regionally, biostratigraphical data from across the Danian-Selandian (D/S) boundary are numerous across a range of localities, including: Egypt (e.g. Faris & Farouk 2012; Farouk & Faris, 2013; Kasem *et al.* 2017, 2022; Faris *et al.* 2023; Farouk *et al.* 2023; Bazeen *et al.* 2024); Egypt and Tunisia (Sprong *et al.* 2013), Tunisia (e.g. Sprong *et al.* 2009; Karoui-Yaakoub *et al.* 2014); Italy (e.g. Coccioni *et al.* 2019); Spain (Arenilas *et al.* 2008; Bernaola *et al.* 2009; Zumaia GSSP, Schmitz *et al.* 2011.); and, France (Steurbaud & Sztrákos 2008). Nevertheless, studies documenting palaeoenvironmental changes using calcareous nannofossil assemblages across the D/S boundary are very rare. These include records from the Weddell Sea, Maud Rise, ODP Site 690 (Bralower 2002), South

Atlantic ODP Site 1262 (Monechi *et al.* 2013), and recently two studies from Egypt: the Wadi El-Maheer section, North Eastern Desert (Metwally 2019) and Gebel Nezzazat, Central Sinai (Kasem *et al.* 2022).

As such, the main aims of this study, based on samples from the Ekma section, west central Sinai (Egypt), are to: (1) document and integrate calcareous nannofossil biostratigraphy and bioevents around the D/S boundary using carbon ($\delta^{13}\text{C}$) and oxygen ($\delta^{18}\text{O}$) isotope data; (2) identify, discuss, and correlate the nature of calcareous nannofossil bioevents across the D/S boundary vis-à-vis their global occurrences; and (3) infer changes in calcareous nannofossil distribution patterns, and infer the depositional environment across the D/S boundary.

Material and methods

Thirty-one samples were analysed at an interval of 20 cm from the 6 m-thick upper Dakhla Formation at the Ekma section, west central Sinai, Egypt (latitudes 28° 43' 15.3" and longitudes 33° 15' 4.2") (Fig. 1A, B). The smear slide technique, following Perch-Nielsen (1985), from unprocessed sediment samples were used for preparing calcareous nannofossil slides. These were then inspected under a light photomicroscope with a 1250 x magnification. On each slide at least 300 specimens were counted to determine the abundance of calcareous nannofossils. The abbreviations used here are LO: Lowest Occurrence, LCtO: Lowest Continuous Occurrence, and HO: Highest Occurrence.

The calcareous nannofossils are categorized based on their ecological strategies (K- and R-mode), water-mass preferences, and trophic regimes (i.e., from warm and oligotrophic to cool and eutrophic) (see Appendix). The calcareous nannofossil diversity is inferred using three parameters: species richness (i.e. the number of taxa), Shannon diversity index (Shannon H), and species dominance. Shannon H is the measure of heterogeneity; a way to measure species diversity within a community, where higher values reflect higher diversity of species within a specific community. Species dominance is the percent of the assemblage composed of the single most abundant species within an assemblage (population) (Walton 1964). The Environmental Isotope Laboratory at the University of Arizona conducted the bulk isotope analysis of carbonate carbon ($\delta^{13}\text{C}$) and oxygen ($\delta^{18}\text{O}$) using a gas-ratio mass spectrometer. Samples were calibrated using the international standard NBS-19. The results showed an average measurement precision of over 0.08 for $\delta^{13}\text{C}$ and less than 0.10 for $\delta^{18}\text{O}$.

Lithostratigraphy

At the Ekma Plateau, the Paleocene succession includes three formations, the upper part of the Dakhla, entire Tarawan, and the lower part of Esna (see Fig. 1B). The Dakhla Formation consists of variegated shales (grey, black, brown, and greenish yellow) in the lower part, and grey marls in the upper part. The ~2 m-thick Tarawan Formation is made up of yellow marls with chert bands that towards the top, changes into chalky limestones. The Esna Formation is mainly composed of green-grey or dark-grey shales with limestone bands with a few gypsum veins. Only the 7 m-thick upper portion of the Dakhla Formation is the subject of the this research (Fig. 1B).

Results

Nannofossil biostratigraphy

In this study, abundant to frequent and moderate to well-preserved calcareous nannofossils are noted, and based on the biozonation of Martini (1971) and Varol (1989), encompasses NP3–NP5 zones (Fig. 2). The LO of and *Chiasmolithus danicus* defines the NP3 Zone (Fig. 2). The base and top of the NP4 Zone is defined by the LOs of *E. macellus* and *Fasciculithus tympaniformis*, respectively (Fig. 2). The NP4 Zone, following the zonation of Varol (1989), is divided into six sub-zones, NTP6, NTP7A-B, and NTP8A-8C (Fig. 2).

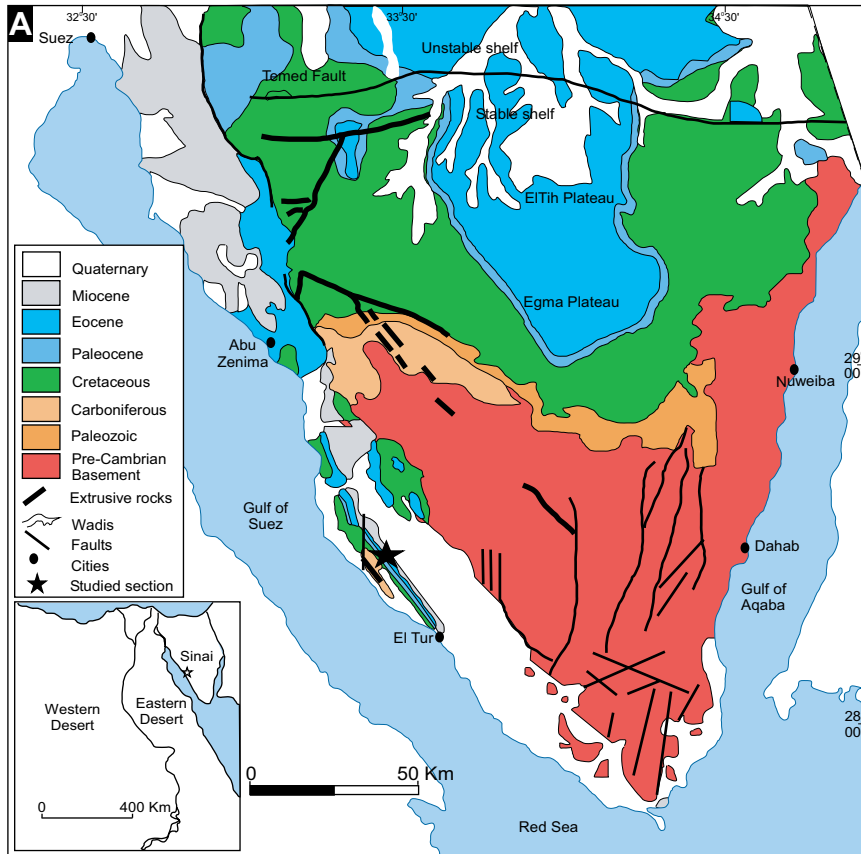
The NP3/NP4 boundary is marked by a hiatus as reflected by the absence of marker species *Hornbrookina edwardsii*, *Prinsus martinii*, *Neocrepidolithus fossus*, and *N. cruciatus* (see also Faris & Farouk 2012). The NTP7A Subzone is defined by the HO of *Neochiastozygus imbrii* (in sample 76) to the LO of *C. edentulus* (in sample 79) (Fig. 2). The LO of *Ch. edentulus*, as also reported by Varol (1989), indicates the base of the NTP7B Subzone (sample 79) (Fig. 2). The interval between the LCtO of *Sphenolithus primus* and the LO of *Lithyptychius ulii* distinguishes the NTP8A Subzone (see Varol 1989; Monechi et al. 2013; Fig. 2). The NTP8B Subzone extends from the LOs of *L. ulii* to that of *L. janii* (Fig. 2). The LO of *L. janii* (in sample 93) and the LO of *F. tympaniformis* distinguishes the NTP8C Subzone (Fig. 2). The LO of *F. tympaniformis* (sample 96) marks the base of the NP5 Zone, whereas its top cannot be determined as the marker of the NP6 Zone, *Heliolithus kleinpellii*, is not recorded (Fig. 2). Some of the representative calcareous nannofossil species are illustrated in Figure 3.

Nannofossil bioevents

Several nannofossil bioevents are identified within the NP4 Zone, enabling reliable correlation with global sequences (Fig. 4). These are briefly enumerated below.

LO and LCtO of Sphenolithus primus.– The base of NTP8 Subzone is defined by the LO of *S. primus* (Varol, 1989). However, Quillévéré et al. (2002) utilized it to subdivide it into two subzones, NP4a and NP4b. In the present work, within the NTP6 Subzone, rare occurrences of *S. primus* are also noted in the initial part of its range, and its LCtO is used here to approximate the base of NTP8A (sample 83; Fig. 2).

Chiasmolithus edentulus.– The Tethys and Zumaia (GSSP-Spain) sections can be correlated with the this



Age	Sinai	Southern Galala	Farafra	Nile Valley	Garra El-Arbian
Ypresian	Egma Fm., Thebes Fm.	Southern Galala Fm.	Farafra Fm.	Thebes Fm.	Dungai Fm.
Thanetian	Tarawan Fm.	Galala Fm.	Maqit M., Eana Shale Fm., An Daba Fm.	Eana Shale Fm., Dababyia Bed.	Garra Fm.
Selandian	Dakhla Fm.	Tectonically	Tarawan Chalk Fm.	Hiatus, Dakhla Fm., Upper Kharga Shale unit.	Kurkur Fm.
Danian	study interval	paleohighs	Bekda (Shale) Member.	Dakhla Fm. or equivalent, Bekda (Shale) Member.	Kurkur Fm.
Maas.	Sudr Chalk Fm.	Unconformity surface	Khoman Chalk Fm.	Hiatus, Dakhla Fm., Lower Kharga Shale unit, Mawhoob Shale and Beris Mudstone members.	

	Limestone		Argillaceous chalky limestone		Conglomerate		Ferruginous Planktic foraminifera		Operculines
	Limestone with chert		Dolostone		Clay		Benthic foraminifera		Nummulites
	Argillaceous limestone		Shale		Sandstone		Ds Da1		Alveolines
	Bivalves		Burrow structure		Unconformity surface		Eg.Da-1		Sequence boundary
	Gastropods		Transgressive system tract		Highstand systems tract		Maximum flooding surface		Ferriband

Fig. 1. A, location Map of Ekma section, West Central Sinai, Egypt. B, Upper Cretaceous-Lower Eocene lithostratigraphy. Figure shows the lithostratigraphical correlation of Upper Cretaceous-Lower Eocene rocks in different places in Egypt.

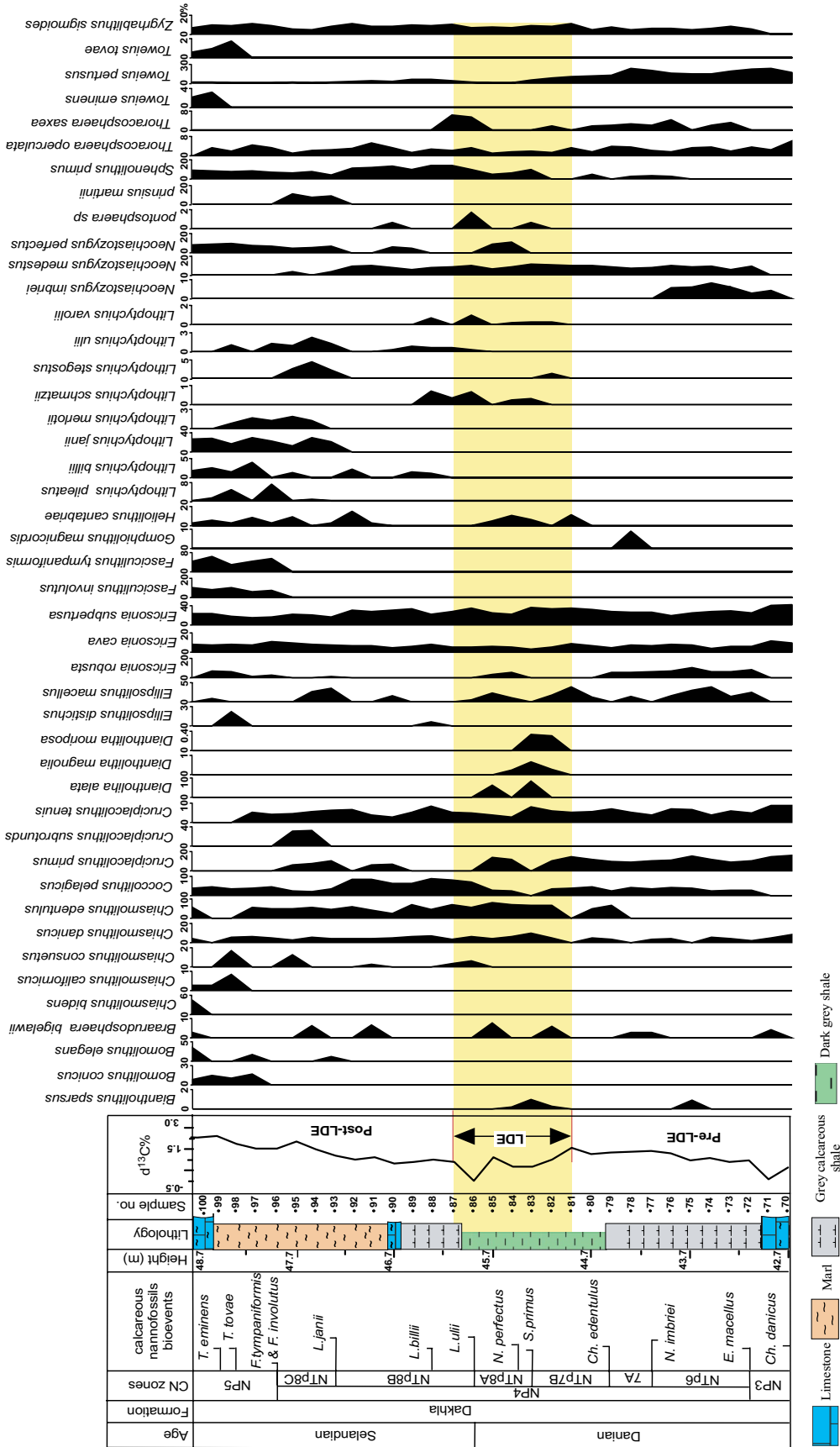


Fig. 2. Litho- and calcareous nannofossil biostratigraphy and bioevents at Ekma section, West Central Sinai, Egypt.

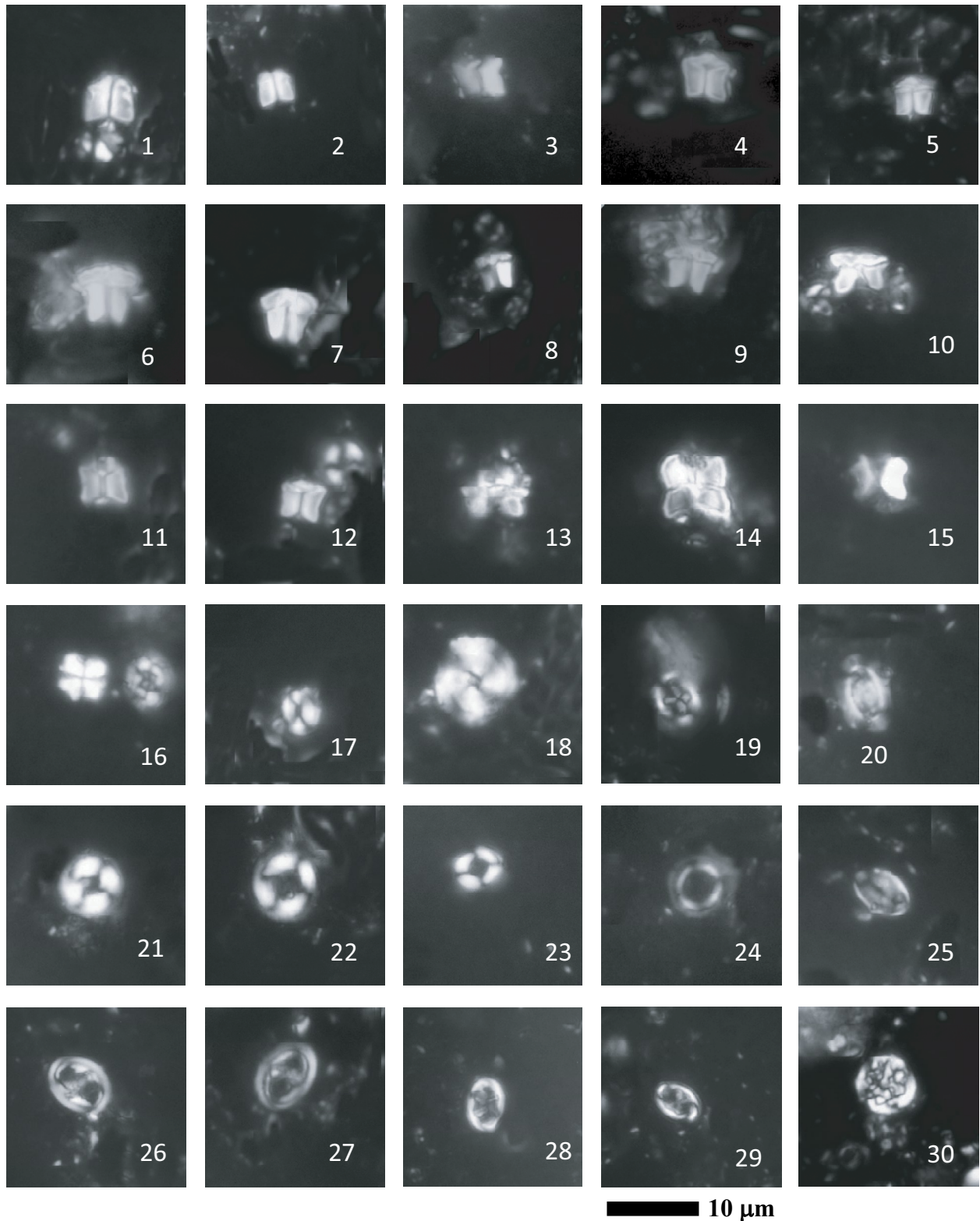


Fig. 3. Important representative calcareous nannofossil species from this study. 1, 2, *Fasciculithus involutus*, sample 98. 3, *Fasciculithus tympaniformis*, sample 96. 4, 5, *Lithoptychius jani*, sample 98. 6, 7, *Lithoptychius merloti*, sample 94, 97. 8–10, *Lithoptychius stegastos*, sample 94, 96, 87. 11, 12, *Lithoptychius ulii*, sample 98, 97. 13, *Lithoptychius schmitzii*, sample 86. 14, *Diantholitha mariposa*, sample 79. 15, *Lithoptychius billii*, sample 86. 16, *Sphenolithus primus*, sample 93. 17, *Ericsonia cava*, sample 85. 18, *Heliolithus cantabriae*, sample 101. 19, *Chiasmolithus danicus*, sample 93. 20, *Ellipsolithus macellus*, sample 79. 21–23, *Ericsonia subpertusa*, sample 73. 24, *Ericsonia robusta*, sample 76. 25, *Pontosphaera* sp., sample 76. 26, 27, *Zeugrhabdotus sigmoides*, sample 74. 28, 29, *Neochiastozygus modestus*, sample 82, 76. (30) *Thoracosphaera saxea*, sample 79.

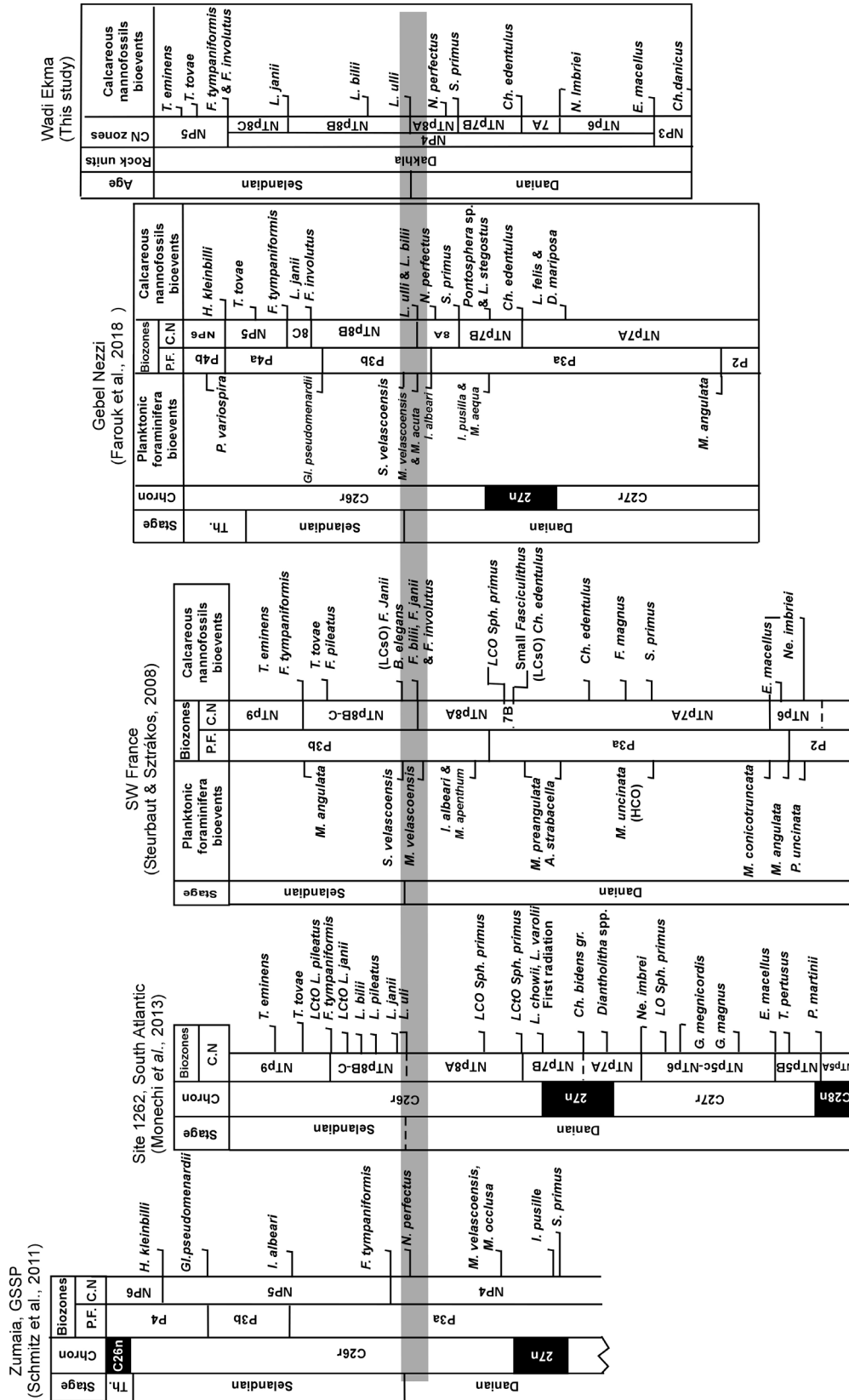


Fig. 4. Correlation between bioevents and magnetostratigraphy of GSSP at Zumaia, Site 1262 at South Atlantic, SW France, Gebel Nezzi and the Ekma sections (the grey line corresponds to the beginning of Latest Danian Event).

study using the LO of *C. edentulus*, which marks the NTP7B base (Bernaola et al. 2009; Monechi et al. 2013; Farouk and Faris, 2013; Metwally, 2019). Here, the LO of *Ch. edentulus* (in sample 79) delineates the base of NTP7B; the species is continuously present from samples 79 to 100 (Fig. 2).

Lithoptychius.— The first taxon to appear in the *Lithoptychius* lineage is the small form of *L. varolii*; it represents the first diversification event of this genus (Monechi et al. 2013). *L. varolii* initially appears at the base of NTP7B Subzone both at Zumaia (Monechi et al. 2013) and at the Wadi El Maheer section, Egypt (Metwally, 2019). The LO of *L. varolii*, is reported in the uppermost part of the NTP7B Subzone (sample 82) (Fig. 2). *Lithoptychius* is well diversified within NTP7B; *L. stegostus* first appears within this subzone (Fig. 2). In the Tethyan region, the LO of *L. schmatzii* is regarded as a reliable event and represents the first radiation of *Lithoptychius*. At Zumaia (Spain) and Qreiya (Egypt) sections, the LO of *L. schmatzii* is at the base of the NTP8A Subzone. Here, the LO of *L. schmatzii* is at the base of NTP8A (Fig. 2). The LO of *L. billii* is noted at the base of the NTP8B Subzone (following Varol, 1989). Nevertheless, its LO is delayed, and appears within the NTP8B Subzone (in sample 88) (Fig. 2). It is noted that with respect to the LO of *Lithoptychius pileatus*, *L. janii*, and *Fasciculithus involutus*, several discrepancies exist with the zonation of Varol (1989) and Agnini et al. (2007 a-b). These discrepancies may well be due to differing taxonomic interpretations. In the zonal scheme of Varol (1989), *L. pileatus* and *L. janii* first appear at the base of the NTP8C Subzone. However, the LO of *L. pileatus* is delayed, as it first occurs within the NTP8C Subzone, in sample 94 (Fig. 2).

Fasciculithus.— The LO *Fasciculithus involutus* is noted at the base of NTP8C (Varol, 1989), though it is delayed; it appears first at the base of the NP5 Zone in sample 96 (Fig. 2).

Carbon and oxygen isotopes

The $\delta^{13}\text{C}$ and $\delta^{18}\text{O}$ isotopic records are useful for tracking changes in biogenic and oceanic environments and water palaeotemperatures, and for determining the age and origin of rocks (d'Hondt & Zachos 1993; Charisi & Schmitz 1995). However, they are also affected by changes in salinity, biological fractionation, diagenesis, and alterations in the global carbon and oxygen budgets, making it difficult to align concepts in isotope stratigraphy (Baum et al. 1994). The oxygen isotope values, in particular, are more susceptible to

post-depositional changes (diagenesis) as compared to carbon isotope values. As a result, interpreting palaeotemperature records from $\delta^{18}\text{O}$ can be tricky, although trends and the magnitude of alterations are generally better preserved (Sexton et al. 2006). In general, $\delta^{13}\text{C}$ is considered to be largely unchanged, and thus appropriate for regional correlation.

In this study, the cross-plot between $\delta^{13}\text{C}$ and $\delta^{18}\text{O}$ shows a weak correlation ($R^2 = 0.4038$), and slight co-variance, and thus indicative of minimal diagenesis (Fig. 5). Broadly, the $\delta^{13}\text{C}$ and $\delta^{18}\text{O}$ values range between -0.05 to $+2.06\text{‰}$ for $\delta^{13}\text{C}$ and -4.32 to -1.98‰ for $\delta^{18}\text{O}$ (Fig. 6). The $\delta^{13}\text{C}$ curve begins at 0.57‰ and drops to 0.03‰ at sample 71. Upwards, the $\delta^{18}\text{O}$ curve starts at -3.88‰ and then decreases to -4.32‰ at sample 71, within the calcareous nannofossil NP3 Zone (Fig. 6). Subsequently, there is a gradual increase in $\delta^{13}\text{C}$ values to 1.49‰ at sample 81 and an increase in $\delta^{18}\text{O}$ to -2.37‰ at sample 81, continuing into the calcareous nannofossil zones NTP6, NTP7A, and the lower part of the NTP7B Subzone (Fig. 6). An abrupt decrease in $\delta^{13}\text{C}$ and $\delta^{18}\text{O}$ values occurs at sample 84 (from 1.49 to 0.62‰ and -2.37 to -4.29‰ respectively), followed by another sudden excursion from samples 85 to 86 (1.06 to -0.05‰ and -2.79 to -3.74‰ in $\delta^{13}\text{C}$ and $\delta^{18}\text{O}$ values, respectively).

This corresponds to the latest Danian Event (LDE), occurring at the boundary between Chron C27n and C26r (topmost calcareous nannofossil NTP7B and NTP8A) (Fig. 6). Two negative $\delta^{13}\text{C}$ excursions are identified, characterized by distinctive double-peak

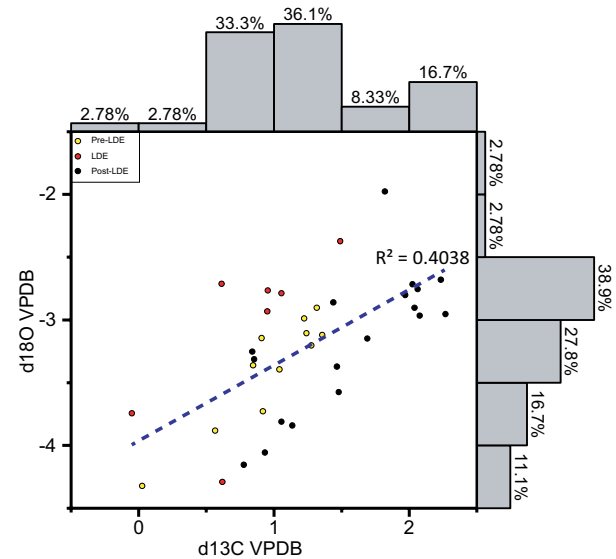


Fig. 5. Histogram showing X-Y scatter plot of $\delta^{13}\text{C}$ versus $\delta^{18}\text{O}$. This plot yields a weak linear relationship ($R^2 = 0.38$) suggesting some diagenesis of the primary $\delta^{13}\text{C}$ signal particularly for the data points of the pre-LDE interval.

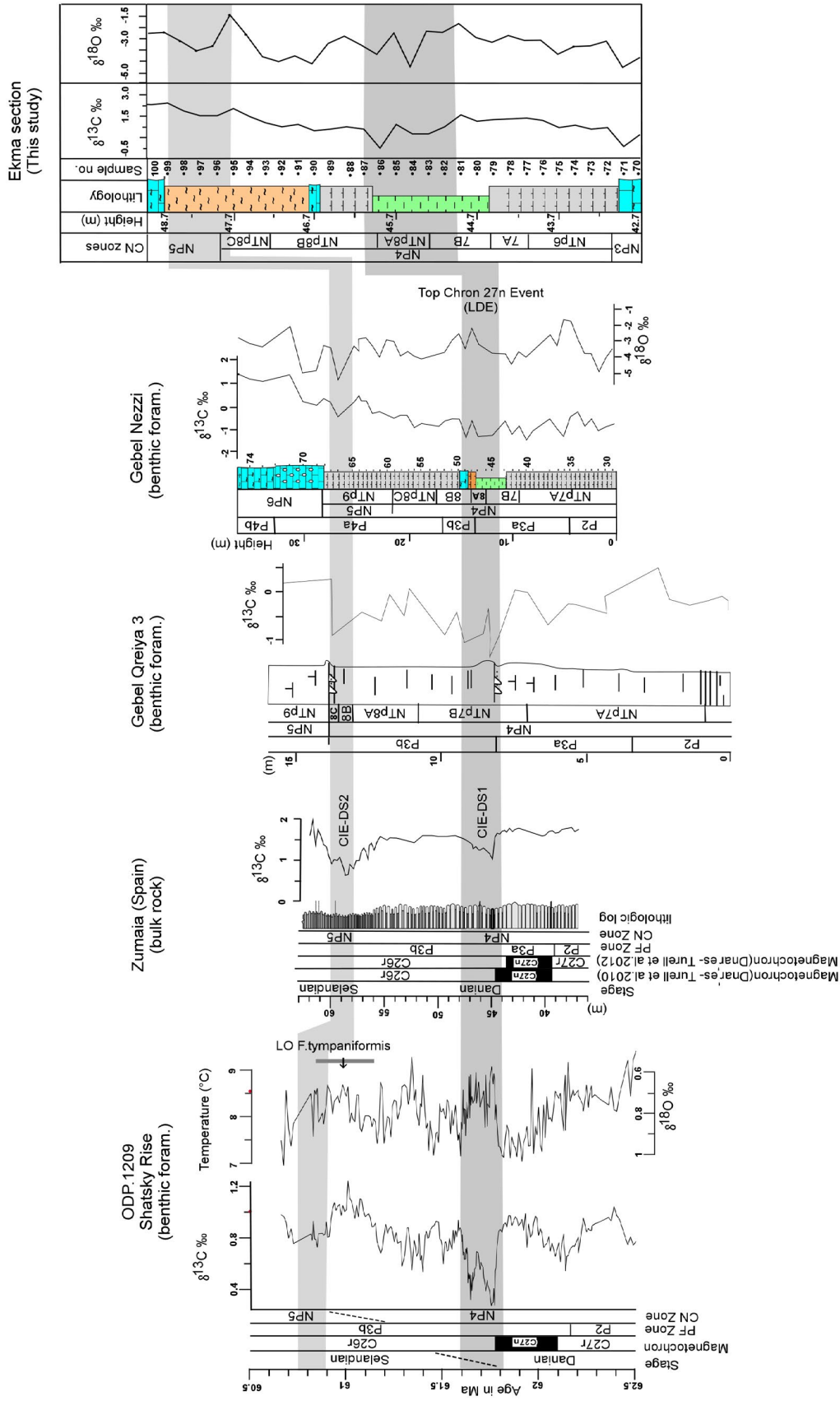


Fig. 6. Carbon isotope correlation of the Ekma section with the Central Pacific (ODP Site 1209; Westerhold et al. 2011), Zumaia (Spain; Arenillas et al. 2008), and Gebel Qreiya in the Nile Basin (Egypt; Bornemann et al. 2009) and Gebel Nezzi (Egypt; Farouk et al. 2018). Grey shaded area represents the global correlation between the two negative excursions.

$\delta^{13}\text{C}$ excursions and sudden decreases in $\delta^{13}\text{C}$ and $\delta^{18}\text{O}$ values. This event correlates with the LDE at the Chron C27n/C26r boundary and the planktic foraminiferal P3a/P3b subzonal boundary at Gebel Nezzi (Luxor) (Farouk *et al.* 2018) (Fig. 6). There is a gradual increase in $\delta^{13}\text{C}$ values reaching 1.82‰ at sample 95, with $\delta^{18}\text{O}$ oscillating to -1.98 ‰ at sample 95, correlating with the calcareous nannofossil NTp8B and NTp8C subzones. Within the calcareous nannofossil NP5 Zone, a short-lived negative $\delta^{13}\text{C}$ and $\delta^{18}\text{O}$ excursion reaches 1.48‰ and -3.58 ‰ at sample 97.

Calcareous nannofossils

Three intervals are noted: pre-LDE (samples 70–80), LDE (samples 81–87), and post-LDE (samples 88–100) (see Fig. 7). Three genera dominate: *Ericsonia* (31%; *E. subpertusa* makes up 66% of the total *Ericsonia* population), *Cruciplacolithus* (13%; *C. tenuis*: 40%), and *Neochiastozygus* (10%; *N. medestus*: 65%) (Fig. 7). In terms of species distribution, *E. subpertusa* is relatively abundant in all three intervals: pre-LDE (17%), LDE (23%), and post-LDE (21%). It is associated with increasing values of *Toweius pertusus*, *Cruciplacolithus primus*, and *Neochiastozygus medestus* and decreasing values of *Zygrhablithus sigmoides*, *Ericsonia cava*, and *Sphenolithus primus* (see Table 1).

Species diversity

In general, the average values for both species richness (i.e., the number of taxa) and Shannon diversity index (Shannon H) gradually increases from the pre-LDE (13 and 2.2, respectively) to LDE (17 and 2.4) and to post-LDE (18 and 2.6) intervals (see Table 1). In contrast, species dominance remains low and gradually decreases; pre-LDE (0.13), LDE (0.12) and post-LDE (0.09) (see Table 1).

Discussion

Diagenesis

The cross-plot between $\delta^{13}\text{C}$ and $\delta^{18}\text{O}$ provides a window to infer possible diagenesis (see Fig. 5). Here, this cross-plot yields a weak linear relationship ($R^2 = 0.4038$) suggesting minimal diagenesis (Fig. 5). Additionally, the present isotope data faithfully reflects the general global trend, such as the double-peak carbon isotope excursion indicating the presence of LDE (see Monechi *et al.* 2013) (see Fig. 6). Additionally, another short-lived, negative $\delta^{13}\text{C}$ and $\delta^{18}\text{O}$ excursion (the CIE-DS2) noted in Egypt (Bornemann *et al.*

2009), Zumaia, Spain (Arenillas *et al.* 2008), and in the Central Pacific (Westerhold *et al.* 2011) is also recorded (Fig. 6). Minimal dissolution is also confirmed by a similar pattern of high species diversity and moderate to well-preserved calcareous nannofossil species (see Fig. 3). In terms of species composition, it has been noted that the absence of small *Prinsius* and high abundances of *C. pelagicus* and *E. subpertusa* are suggestive of increased dissolution (see Samtleben & Schoreder 1992; Monechi *et al.* 2013). *Prinsius* occurs only in three samples within the post-LDE event (samples 93–95), and the abundance of *C. pelagicus* remains relatively low (2.4–3.9%) but *E. subpertusa* is one of the dominant species (see Table 1). However, the presence of moderate to well-preserved calcareous nannofossil species and low species dominance throughout the study interval (see Fig. 7) suggests minimal dissolution.

First radiation of the fasciculiths

At Zumaia (Spain), the first radiation of *Fasciculithus* occurs very close to the base of NTp7B Subzone (Steurbaut & Sztrákos 2008; Monechi *et al.* 2013). At Site 1262, it occurs within the upper part of the NTp7B Subzone (LOs of *Lithoptychius chowii*, *L. varolii*; see Monechi *et al.* 2013). At the Qreiya section (Egypt), the first appearance of *L. chowii* and *L. varolii* occurs within the lower part of the NTp7A Subzone (Monech *et al.* 2013), whereas in the northern Eastern Desert (Wadi El-Maheer section), this event is noted at the topmost part of the NTp7A Subzone (Metwally 2019). Here, *Diantholitha magnolia*, *D. mariposa*, *L. varolii*, and *L. stegostus* first occur in the topmost part of the NTp7B Subzone (sample 82) (see Fig. 2).

Aubry *et al.* (2011) introduced two new genera, *Diantholitha* and *Lithoptychius* based on the morphological structure of the family Discoasterales; this classification is also used in here. At the top of the NTp7B Subzone, *D. magnolia* occurs with LOs of *L. varolii* and *L. stegostus*. The LOs of *Diatholitha* (*D. mariposa*, *D. hemisphaerica*) is followed upward by the LOs of *Lithoptychius* (*L. chowii*, *L. felis*, and *L. stegostus*) within the NTp7B Subzone (Aubry *et al.* 2012). *D. magnolia* and *D. mariposa* first occur prior to the LOs of *L. chowii* and *L. varolii* (Monechi *et al.* 2013). In Tethyan sections these are recorded after the appearance of *L. schmitzii*, characterized by the absence of fasciculiths (*Lithoptychius*) (Monechi *et al.* 2013). The NTp8A Subzone has a reduced thickness (~1 m thick), and hence, the paracme interval of fasciculiths is represented only by one sample (sample 85, ~20 cm thick); this is marked by the absence of *Lithoptychius*.

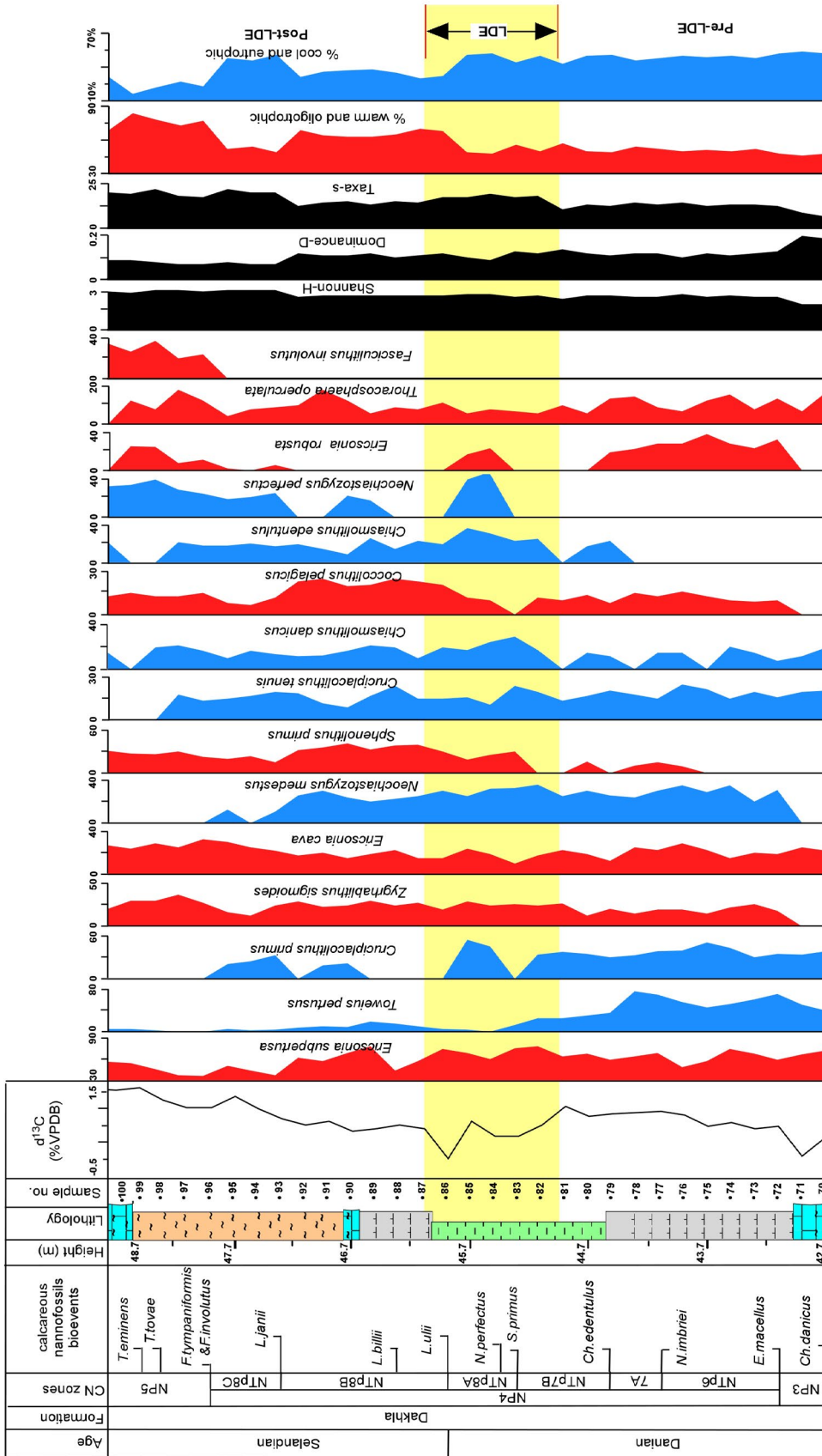


Fig. 7. Proxies used to infer the palaeoenvironments.

Second radiation of the fasciculiths

The end of the paracme of fasciculiths is characterized by the radiation of *Lithoptychius* and *Fasciculithus*. At Site 1262, Qreiya and Zumaia sections, the LO of *L. ulii* and the LRO of *L. jani* has been used to delineate the base of NTp8B-C subzones (the second radiation of fasciculiths) (Monechi *et al.* 2013). Alegret *et al.* (2016) at Caravaca (Spain) used the LO of *L. ulii* within NTp8 Zone to delineate the second radiation of fasciculiths. At Gebel Nezzazet, west central Sinai, the second radiation of fasciculiths is characterized by the LOs of *L. ulii* and *L. billi*, at the base of NTp8B Subzone (Faris *et al.* 2023). Here, this radiation also occurs at the base of NTp8B Subzone (sample 86) and is marked by the LO of *L. ulii*. However, the LO of *L. jani* (sample 93) occurs at the base of the NTp8C Subzone.

Calcareous nannofossil distribution: global and local comparisons

Pre-LDE interval.– During the pre-LDE interval, cool and eutrophic conditions are noted as reflected by the abundance of cool water taxa of *Toweius pertusus* and *Cruciplacolithus primus* (Bukry 1973; Bralower 2002) (Fig. 7). Metwally (2019) observed similar conditions, but with a gradual warming towards the end of the pre-LDE interval at the Wadi El-Maheer section. These cooler conditions coincided with lowered sea

levels and increased terrigenous input, due to the shallower palaeodepth at the Wadi El-Maheer section, as reflected by the record of fish remains suggesting closer proximity to shorelines. Increased *Neochiastozygus* abundance reflect elevated nutrient levels, attributed to sea-level changes influencing nutrient fluxes (Mutterlose *et al.* 2007; Self-Trail *et al.* 2012).

LDE Interval.– In terms of species distribution patterns, this interval is characterized by maximum abundances of warm and oligotrophic species such as *Ericsonia subpertusa*, and associated increased abundances of *Sphenolithus primus* and *Zygrhablithus sigmoides* (Table 1). Increased nutrient availability is also noted here, as reflected by the higher relative abundance of *Neochiastozygus* (Mutterlose *et al.* 2007; Self-Trail *et al.* 2012; see Table 1). Overall, across the LDE, there is a general warming of surface waters across the LDE with increased warmth at the later stages and a corresponding decline if cool water taxa (see Fig. 7). Metwally (2019) also noted warmer, oligotrophic and relatively unstable environmental conditions across the LDE. Other studies, based on $\delta^{13}\text{C}$ excursions and associated nannofossil assemblages, have suggested a transition to increased sea levels and a transgressive phase, with increased warmth and nutrient availability in oceanic waters across the LDE (Arenillas *et al.* 2008; Westerhold *et al.* 2011). Local species diversity remains relatively stable with low dominance (Metwally 2019; Kasem *et al.* 2022).

Table 1. Distribution of calcareous nannofossils in the identified intervals (pre-LDE, LDE and post-LDE).

Species (5)	<i>Ericsonia subpertusa</i>	<i>Toweius pertusus</i>	<i>Cruciplacolithus primus</i>	<i>Zygrhablithus sigmoides</i>	<i>Ericsonia cava</i>	<i>Neochiastozygus medestus</i>	<i>Sphenolithus primus</i>	Taxa	Shannon H	Dominance
post-LDE	21	3	4	10	9	4	11	18	2.6	0.09
LDE	23	4	8	8	6	10	7	17	2.4	0.12
pre-LDE	18	15	10	4	6	7	1	13	2.2	0.13

Genus (%)	<i>Ericsonia</i>	<i>Cruciplacolithus</i>	<i>Neochiastozygus</i>	<i>Chiasmolithus</i>	<i>Toweius</i>
post-LDE	35	19	8	5	17
LDE	30	13	13	12	4
pre-LDE	27	8	10	10	3

Globally, the LDE resembles the Paleocene-Eocene Thermal Event (PETM) and is marked by increased abundances of warm, oligotrophic taxa (Bralower 2002; Tantawy 2009; Metwally 2019). The inclusion of the First and Second Radiations of *Fasciculithus* at different subzones during the LDE suggests that diachronism, possibly influenced by regional bathymetric changes (Self-Trail et al. 2012; Bralower 2002; Gibbs et al. 2006b). The varying timing of these radiations across different locations reflects regional differences in oceanographic conditions and bathymetry that severely affected the distribution and evolution of calcareous nannofossil species (Arenillas et al. 2008; Monechi et al. 2013). This diachrony also highlights the complex interplay between local environmental factors and global climatic events during the LDE.

The D/S boundary, as defined by the LO of *L. ulii* at the base of the NTp8B Subzone (Bernaola et al. 2009; Monechi et al. 2013), corresponds to significant sea-level changes. The boundary is associated with a transgressive phase, which is reflected in the shift towards warmer, oligotrophic conditions in the post-D/S boundary interval (Fig. 7). This transgression is consistent with global sea-level rise and increased warmth observed at the base Selandian (Hardenbol et al. 1998; Haq 2015; Farouk 2016).

Post-LDE interval.– The post-LDE interval is marked by an increase in the relative abundances of *Zygrhablithus sigmoides* and *Sphenolithus primus* (Fig. 7; Table 1). *Zygrhablithus*, a deep-water taxon, thrives in oligotrophic environments, while *Sphenolithus* and *Fasciculithus* (notably increasing at the interval's end; Fig. 7) are adapted to warmer conditions (Wei & Wise 1990; Bralower 2002). Additionally, with in the post-D/S boundary interval, in particular the NTp8B Zone, increased relative abundances of warm water taxa, *Ericsonia subpertusa*, *Coccolithus pelagicus*, *Sphenolithus primus*, and *Thoracosphaera operculata* and in general of warm water taxa are noted (see Fig. 7). At the Wadi El-Maheer section also, the post-LDE is characterized by warmer, oligotrophic environments, but with a notable presence of *Prinsius* (Metwally 2019). Both Wadi El-Maheer and Wadi Ekma sections reflect increased species richness and diversity during the post-LDE interval, alongside a reduction in species dominance, suggesting improved conditions. This is corroborated by the increased abundance of *Cruciplacolithus* (Table 1), which indicates stable marine conditions and supports the notion of a continued transgressive phase (Tantawy 2003; Farouk 2016).

Here, it must be mentioned of an abrupt rise in relative abundance of the warm water taxa which starts

at the NP5 Zone (at sample 96; see Fig. 7), rise and dominance of *Fasciculithus involutus*, and with consistently higher values of $\delta^{13}\text{C}$ suggesting oligotrophic conditions but with increased species diversity and low species dominance suggesting fairly stable conditions (see Fig. 7). Metwally (2019), who did not differentiate *Fasciculithus* into individual species, also recorded increased presence of *Fasciculithus* spp. within the NP5 Zone.

Conclusions

The following conclusions may be drawn from this study:

1. The Ekma section, west central Sinai (Egypt) records three calcareous nannofossil zones, NP3, NP4, and NP5. This is the first nearly complete section from Egypt, straddling the D/S boundary.
2. The first negative $\delta^{13}\text{C}$ excursion occurs during the LDE, and within NTp7B and NTp8A subzones. The second negative excursion occurs within the NP5 Zone, and close to the top of the Dakhla Formation.
3. The pre-LDE interval is characterized by cool and eutrophic conditions and dominated by the relative abundances of *Toweius pertusus* and *Cruciplacolithus primus*.
4. The LDE is distinguished by the maximum relative abundances of warm and oligotrophic species – *Ericsonia subpertusa*, *Sphenolithus primus*, and *Zygrhablithus sigmoides*.
5. The interval of post-LDE is marked by the relative abundance of *Z. sigmoides* and *S. primus* suggestive of deeper conditions with warm and oligotrophic species.
6. Species richness and Shannon H gradually increase from the pre-LDE to LDE to the post-LDE interval whereas a corresponding decline in species dominance, which remains low, is noted suggesting a gradual improved in environmental conditions.

Acknowledgments.– We thank the editor, Dr Gabriela Mangano, and two anonymous reviewers for improving the manuscript and providing useful comments. Fayez Ahmad is gratefully acknowledged for his financial support of this work provided by the Hashemite University.

References

- Agnini, C., Fornaciari, E., Raffi, Rio, D., Röhl, U. & Westerhold, T. 2007a. High-resolution nannofossil biochronology of the middle Paleocene to early Eocene at ODP Site 1262: implications for calcareous nannoplankton evolution *Marine Micropaleontology* 64, 215–248. <https://doi.org/10.1016/j.marmicro.2007.05.003>
- Agnini, C., Fornaciari, E., Rio, D., Tateo, F., Backman, J. & Giusberti, L. 2007b. Responses of calcareous nannofossil assemblages, mineralogy and geochemistry to the environmental perturbations across the Paleocene/Eocene boundary

- in the Venetian Pre-Alps. *Marine Micropaleontology* 63, 19–38. <https://doi.org/10.1016/j.marmicro.2006.10.002>
- Algret, I., Ortiz, S., Arreguin, G., Monchi, S. & Milina, E. 2016. Microfossil turnover across the uppermost Danian at Caravaca, Spain: Paleoenvironmental inferences and identification of the latest Danian event. *Palaeogeography, Palaeoclimatology, Palaeoecology* 463, 45–59. <https://doi.org/10.1016/j.palaeo.2016.09.013>
- Arenillas, I., Molina, E., Ortiz, S. & Schmitz, B. 2008. Foraminiferal and $\delta^{13}\text{C}$ isotopic event stratigraphy across the Danian–Selandian transition at Zumaya (northern Spain): chronostratigraphic implications. *Terra Nova* 20, 38–40. <https://doi.org/10.1111/j.1365-3121.2007.00784.x>
- Aubry, M.-P. 1998. Early Paleogene calcareous nannoplankton evolution: A tale of climatic amelioration, 158–203. In: Aubry, M.-P., Lucas, S.G. & Berggren, W.A. (eds), *Late Paleocene-Early Eocene Climatic and Biotic Events in The Marine and Terrestrial Records*. Columbia University Press, New York.
- Aubry, M.P., Bord, D. & Rodriguez, O. 2011. New taxa of the Order Discoasterales Hay 1977. *Micropaleontology* 57, 269–287. <https://doi.org/10.47894/mpal.57.3.06>
- Aubry, M.-P., Rodriguez, O., Bord, D., Godfrey, L., Schmitz, B. & Knox, R. 2012. The First Radiation of the Fasciculiths: Morphological adaptations of the coccolithophores to oligotrophy. *Austrian Journal of Earth Sciences* 105, 29–38.
- Baum, J.S., Baum, G.R., Thompson, P.R. & Humphrey, J.D. 1994. Stable isotope evidence for relative and eustatic sea-level changes in Eocene to Oligocene carbonates, Baldwin County, Alabama. *Geological Society of America, Bulletin* 106, 324–329. [https://doi.org/10.1130/0016-7606\(1994\)106<0824:SIEFRA>2.3.CO;2](https://doi.org/10.1130/0016-7606(1994)106<0824:SIEFRA>2.3.CO;2)
- Bazeen, Y.S., Hewaidy, A.G.A., Samir, A., Moneer, E.S.M., Abd El-Moghny, M.W. & Ayyad, H.M. 2024. Sequence stratigraphy of the Paleocene succession in the Kharga Oasis, Western Desert, Egypt: insights from microplankton biostratigraphy and benthic foraminifer paleoenvironments. *Palaeoworld* 33, 188–204. <https://doi.org/10.1016/j.palwor.2023.01.005>
- Bernaola, G., Martín-Rubio, M. & Baceta, J.I. 2009. New high resolution calcareous nannofossil analysis across the Danian–Selandian transition at the Zumaia section: comparisons with South Tethys and Danish sections. *Geologica Acta* 7, 79–92.
- Bornemann, A., Schulte, P., Sprong, J., Steurbaut, E., Youssef, M. & Speijer, R.P. 2009. Latest Danian carbon isotope anomaly and associated environmental change in the Southern Tethys (Nile Basin, Egypt). *Journal of the Geological Society of London* XX, 1135–1142. <https://doi.org/10.1144/0016-76492008-104>
- Bralower, T.J. 2002. Evidence of surface water oligotrophy during the Paleocene–Eocene Thermal Maximum: nannofossil assemblage data from Ocean Drilling Program Site 690, Maud Rise, Weddell Sea. *Paleoceanography* 17, 13–1. <https://doi.org/10.1029/2001PA000662>
- Bukry, D. 1973. Phytoplankton stratigraphy, Deep Sea Drilling Project Leg 20, Western Pacific Ocean. *Initial Reports DSDP* 20, 307–317. <https://doi.org/10.2973/dsdp.proc.20.114.1973>
- Bukry, D. 1974. Cretaceous and Paleogene coccoliths stratigraphy, DSDP, Leg 26. *Initial Reports DSDP* 26, 669–673. <https://doi.org/10.2973/dsdp.proc.26.129.1974>
- Charisi, S.D. & Schmitz, B., 1995. Stable ($\delta^{13}\text{C}$, $\delta^{18}\text{O}$) and strontium ($^{87}\text{Sr}/^{86}\text{Sr}$) isotopes through the Paleocene at Gebel Aweina, eastern Tethyan region. *Palaeogeography, Palaeoclimatology, Palaeoecology* 116, 103–129. [https://doi.org/10.1016/0031-0182\(94\)00090-U](https://doi.org/10.1016/0031-0182(94)00090-U)
- Coccioni, R., Frontalini, F., Catanzariti, R., Jovane, L., Rodelli, D., Rodrigues, I.M., Savian, J.F., Giorgioni, M. & Galbrun, B. 2019. Paleoenvironmental signature of the Selandian–Thanetian transition event (STTE) and early late Paleocene event (ELPE) in the Contessa Road section (western Neo-Tethys). *Palaeogeography, Palaeoclimatology, Palaeoecology* 523, 62–77. <https://doi.org/10.1016/j.palaeo.2019.03.023>
- D'Hondt, S. & Zachos, J.C. 1993. On stable isotopic variation and earliest Paleocene planktonic foraminifera. *Paleoceanography* 8, 527–547. <https://doi.org/10.1029/93PA00952>
- Dinarès-Turell, J., Stoykova, K., Baceta, J.I., Ivanov, M. & Pujalte, V. 2010. High resolution intra- and interbasinal correlation of the Danian–Selandian transition (Early Paleocene): the Bjala section (Bulgaria) and the Selandian GSSP at Zumaia (Spain). *Paleogeography, Paleoclimatology, Paleoecology* 297, 511–533. <https://doi.org/10.1016/j.palaeo.2010.09.004>
- Dinarès-Turell, J., Pujalte, V., Stoykova, K., Baceta, J.I. & Ivanov, M., 2012. The Paleocene ‘top chron C27n’ transient greenhouse episode: evidence from marine pelagic Atlantic and peri-Tethyan sections. *Terra Nova* 24, 477–486. <https://doi.org/10.1111/j.1365-3121.2012.01086.x>
- Faris, M. & Farouk, S. 2012. Integrated biostratigraphy of the Upper Maastrichtian–Paleocene successions in north-central Sinai, Egypt. *Geologia Croatia* 65, 139–160. <https://doi.org/10.4154/GC.2012.10>
- Faris, M., Shabaan, M., Abdelhady, A.A., Ahmed, M.S. & Shaker, F. 2023. The Paleocene climate in west central Sinai (Egypt): insights from the calcareous nannofossils. *Arabian Journal of Geosciences* 16, 448. <https://doi.org/10.1007/s12517-023-11566-z>
- Farouk, S. 2016. Paleocene stratigraphy in Egypt. *Journal of African Earth Sciences* 113, 126–152. <https://doi.org/10.1016/j.jafrearsci.2015.10.013>
- Farouk, S. & Faris, M. 2013. Calcareous nannofossil and foraminiferal bio-events of the Danian–Selandian transition of the Quseir area, northwestern Red Sea margin, Egypt. *Micropaleontology* 59, 201–222. <https://doi.org/10.47894/mpal.59.2.10>
- Farouk, S., Askalany, M., Ahmad, F., Youssef, M., Taha, S. & El-Sorogy, A., 2018. Micropalaeontological and isotopic analyses of the middle Palaeocene succession at Gebel Nezzi (Luxor, Egypt): Implications for eustatic changes. *Geological Journal* 54(3) 1–19. <https://doi.org/10.1002/gj.3240>
- Farouk, S., Jain, S., Ahmad, F., Abu-Alam, T., Al-Kahtany, K., El Agroudy, I.S., Bazeen, Y.S. & Shaker, F. 2023. Multiproxy analyses of paleoenvironmental and paleoceanographic changes during the Danian–Selandian in East Central Sinai: An integrated stable isotope and planktic foraminiferal data. *Frontiers in Earth Science* 11, 1158991. <https://doi.org/10.3389/feart.2023.1158991>
- Gibbs, S.J., Bown, P.R., Sessa, J.A., Bralower, T.J. & Wilson, P.A. 2006a. Nannoplankton extinction and origination across the Paleocene–Eocene Thermal Maximum. *Science* 314, 1770–1773. <https://doi.org/10.1126/science.1133902>
- Gibbs, S.J., Bralower, T.J., Bown, P.R., Zachos, J.C. & Bybell, L.M. 2006a. Shelf and open ocean calcareous phytoplankton assemblages across the Paleocene Eocene thermal maximum: implications for global productivity gradients. *Geology* 34, 233–236. <https://doi.org/10.1130/G22381.1>
- Haq, B.U. 2014. Cretaceous eustasy revisited. *Global and Planetary Change* 113, 44–58. <https://doi.org/10.1016/j.gloplacha.2013.12.007>
- Haq, B.U. & Lohmann, G.P. 1976. Early Cenozoic calcareous nannoplankton biogeography of the Atlantic Ocean. *Marine Micropaleontology* 1, 119–194. [https://doi.org/10.1016/0377-8398\(76\)90008-6](https://doi.org/10.1016/0377-8398(76)90008-6)
- Hardenbol, J., Thierry, J., Farley, M.B., Jacquin, T., de Graciansky, P.-C. & Vail, P.R. 1998. Mesozoic–Cenozoic sequence chronostratigraphy framework of European basins, 3–14. In: de Graciansky, P.-C., Hardenbol, J., Jacquin, T. & Vail, P.R. (eds), *Sequence Stratigraphy of European Basins*. SEPM Special Publication 60.
- Jiang, S. & Wise, S.W. 2007. A new *Coccolithus* species that thrived during the Paleocene/Eocene Thermal Maximum. *Journal of Nannoplankton Research* 29, 88–91. <https://doi.org/10.58998/jnr2131>
- Karoui-Yaakoub, N., Mtimet, M.S., Negra, M.H., Grira, C. & Gusemi, W. 2014. The registration of the Mid-Paleocene biotic event (MPBE) in Tunisia. *Paleontology Journal* xx, 760436. <https://doi.org/10.1155/2014/760436>
- Kasem, A.M. 2023. Lithostratigraphy, Stable Isotope Stratigraphy and Calcareous Nannofossils Biostratigraphy of the Danian–Thanetian at Nukhul, Sinai, Egypt. *Frontiers in Scientific Research and Technology* 5, 73–83. <https://doi.org/10.21608/frst.2023.178854.1078>

- Kasem, A.M., Wise, S., Jr., Faris, M., Farouk, S. & Zahran, E. 2017. Calcareous nannofossil biostratigraphy of the Paleocene at the Misheiti section, East Central Sinai, Egypt. *Arabian Journal of Geoscience* 10, 455. <https://doi.org/10.1007/s12517-017-3217-4>
- Kasem, A.M., Faris, M., Jovane, L., Ads, T.A., Frontalini, F. & Zaky, A.S. 2022. Biostratigraphy and Paleoenvironmental Reconstruction at the Gebel Nezzazat (Central Sinai, Egypt): A Paleocene Record for the Southern Tethys. *Geosciences* 12, 96. <https://doi.org/10.3390/geosciences12020096>
- Martini, E. 1971. Standard Tertiary and Quaternary calcareous nannoplankton zonation. *Second Planktonic Conference, Proceedings* 2, 739–785.
- Metwally, A.A. 2019. Characterization of the calcareous nannofossil assemblages across the Latest Danian Event (LDE) at Wadi El-Maheer, northern Eastern Desert, Egypt. *Journal of African Earth Sciences* 156, 58–67. <https://doi.org/10.1016/j.jafrearsci.2019.05.008>
- Monechi, S., Reale, V., Bernaola, G. & Balestra, B. 2013. The Danian/Selandian boundary at Site 1262 (South Atlantic) and in the Tethyan region: biomagnetostratigraphy, evolutionary trends in fasciculiths and environmental effects of the Latest Danian Event. *Marine Micropaleontology* 98, 28–40. <https://doi.org/10.1016/j.marmicro.2012.11.002>
- Mutterlose, J., Linnert, C. & Norris, R.D. 2007. Calcareous nannofossils from the Paleocene–Eocene Thermal Maximum of the equatorial Atlantic (ODP Site 1260B): evidence for tropical warming. *Marine Micropaleontology* 65, 13–31. <https://doi.org/10.1016/j.marmicro.2007.05.004>
- Palcu, D.V., Muraszko, J.R., Jaqueto, P.F., Jovane, L. 2020. The birth of a connected South Atlantic Ocean: A Magnetostratigraphic Perspective. *Frontiers in Earth Sciences* 8, 375. <https://doi.org/10.3389/feart.2020.00375>
- Perch-Nielsen, K. 1985. Cenozoic calcareous nannofossils, 427–554. In: Bolli, H.M., Saunders, J.B. & Perch-Nielsen, K. (eds), *Plankton Stratigraphy*. Cambridge Earth Science Series, Cambridge, 11.
- Quillévéré, F., Aubry, M.P., Norris, R.D. & Berggren, W.A. 2002. Paleocene oceanography of the eastern subtropical Indian Ocean: an integrated magneto-biostratigraphic and stable isotope study of ODP Hole 761B (Wombat Plateau). *Palaeogeography, Palaeoclimatology, Palaeoecology* 184, 371–405. [https://doi.org/10.1016/S0031-0182\(02\)00275-4](https://doi.org/10.1016/S0031-0182(02)00275-4)
- Raffi, I., Backman, J., Zachos, J.C. & Sluijs, A. 2009. The response of calcareous nannofossil assemblages to the Paleocene Eocene thermal maximum at the Walvis Ridge in the South Atlantic. *Marine Micropaleontology* 70, 201–212. <https://doi.org/10.1016/j.marmicro.2008.12.005>
- Samtleben, C. & Schröder, A. 1992. Living coccolithophore communities in the Norwegian-Greenland Sea and their record in sediments. *Marine Micropaleontology* 19, 333–354. [https://doi.org/10.1016/0377-8398\(92\)90037-K](https://doi.org/10.1016/0377-8398(92)90037-K)
- Schmitz, B., Asaro, F., Molina, E., Monechi, S., von Salis, K. & Speijer, R.P. 1997. High resolution iridium, $\delta^{13}\text{C}$, $\delta^{18}\text{O}$, foraminifera and nannofossil profiles across the latest Paleocene benthic extinction event at Zumaya, Spain. *Palaeogeography, Palaeoclimatology, Palaeoecology* 133, 49–68. [https://doi.org/10.1016/S0031-0182\(97\)00024-2](https://doi.org/10.1016/S0031-0182(97)00024-2)
- Schmitz, B., Molina, E. & von Salis, K. 1998. The Zumaya section in Spain; a possible global stratotype section for the Selandian and Thanetian stages. *Newsletters on Stratigraphy* 36, 35–42. <https://doi.org/10.1127/nos/36/1998/35>
- Schmitz, B., Pujalte, V., Molina, E., Monechi, S., Orue-Etxebarria, X., Speijer, R.P., Alegret, L., Apellaniz, E., Arenillas, I., Aubry, M.P., Baceta, J.I., Berggren, W.A., Bernaola, G., Caballero, F., Clemmensen, A., Dinarès-Turell, J., Dupuis, C., Heilmann-Clausen, C., Hilario Orús, A., Knox, R., Martín-Rubio, M., Ortiz, S., Payros, A., Petrizzo, M.R., von Salis, K., Sprong, J., Steurbaut, E. & Thomsen, E. 2011. The global stratotype sections and points for the bases of the Selandian (Middle Paleocene) and Thanetian (Upper Paleocene) stages at Zumaya, Spain. *Episodes* 34, 220–243. <https://doi.org/10.18814/epiiugs/2011/v34i4/002>
- Self-Trail, J.M., Powars D.S., Watkins, D.K. & Wandless, G.A. 2012. Calcareous nannofossil assemblage changes across the Paleocene–Eocene Thermal Maximum: evidence from a shelf setting. *Marine Micropaleontology* 92–93, 61–80. <https://doi.org/10.1016/j.marmicro.2012.05.003>
- Sexton, P.F., Wilson, P.A. & Pearson, P.N. 2006. Microstructural and geochemical perspectives on planktic foraminiferal preservation: ‘glassy’ versus ‘frosty’. *Geochemistry, Geophysics, Geosystems* 7, xx–xx. <https://doi.org/10.1029/2006GC001291>
- Sprong, J., Speijer, R.P. & Steurbaut, E. 2009. Biostratigraphy of the Danian/Selandian transition in the southern Tethys, with special reference to the Lowest Occurrence of planktic foraminifera *Igorina albeari*. *Geologica Acta* 7, 63–77.
- Sprong, J., Kouwenhovens, T.J., Bornemann, A., Dupuis, C., Speijer, R.P., Stassen, P. & Steurbaut, E. 2013. In search of the Latest Danian Event in a paleobathymetric transect off Kasserine Island, north-central Tunisia. *Paleogeography, Paleoclimatology, Paleoecology* 379–380, 1–16. <https://doi.org/10.1016/j.palaeo.2013.01.018>
- Stassen, P., Dupuis, C., Morsi, A.M., Steurbaut, E. & Speijer, R.P. 2009. Reconstruction of a latest Paleocene shallow-marine eutrophic paleoenvironment at Sidi Nasseur (Central Tunisia) based on foraminifera, ostracoda, calcareous nannofossils and stable isotopes ($\delta^{13}\text{C}$, $\delta^{18}\text{O}$). *Geologica Acta* 7, 93–112.
- Steurbaut, E. & Sztrákos, K. 2008. Danian/Selandian boundary criteria and North Sea Basin-Tethys correlations based on calcareous nannofossil and foraminiferal trends in SW France. *Marine Micropaleontology* 67, 1–29. <https://doi.org/10.1016/j.marmicro.2007.08.004>
- Tantawy, A.A.M. 2003. Calcareous nannofossil biostratigraphy and paleoecology of the Cretaceous Tertiary transition in the central eastern Desert of Egypt. *Marine Micropaleontology* 47, 323–356. [https://doi.org/10.1016/S0377-8398\(02\)00135-4](https://doi.org/10.1016/S0377-8398(02)00135-4)
- Tantawy, A.A.M. 2009. Lithology, calcareous nannofossils and stable isotope changes across the Paleocene/Eocene thermal maximum at southeast Kharga Oasis, Western Desert, Egypt. *Egyptian Journal of Paleontology* 9, 145–181.
- Tremolada, F. & Bralower, T.J. 2004. Nannofossil assemblage fluctuations during the Paleocene–Eocene Thermal Maximum at Sites 213 (Indian Ocean) and 401 (North Atlantic Ocean): palaeoceanographic implications. *Marine Micropaleontology* 52, 107–116. <https://doi.org/10.1016/j.marmicro.2004.04.002>
- Varol, O. 1989. Paleocene calcareous nannofossil biostratigraphy, 267–310. In: Crux, J.A. & van Heck, S.E. (eds), *Nannofossils and Their Applications*. British Micropaleontology Society Series, 12.
- Walton, W.R. 1964. Recent foraminiferal ecology and paleoecology, 151–237. In: Imbrie, J. & Newell, N. (eds), *Approaches to Paleocology*. Wiley, New York.
- Wei, W. & Wise Jr., S.W. 1990. Biogeographic gradients of middle Eocene-Oligocene calcareous nannoplankton in the south Atlantic Ocean. *Palaeogeography, Palaeoclimatology, Palaeoecology* 79, 29–61. [https://doi.org/10.1016/0031-0182\(90\)90104-F](https://doi.org/10.1016/0031-0182(90)90104-F)
- Westerhold, T., Röhl, U., Raffi, I., Fornaciari, E., Monechi, S., Reale, V., Bowles, J. & Evans, H.F. 2008. Astronomical calibration of the Paleocene Time. *Palaeogeography, Palaeoclimatology, Palaeoecology* 257, 377–403. <https://doi.org/10.1016/j.palaeo.2007.09.016>
- Westerhold, T., Röhl, U., Donner, B., McCarren, H.K. & Zachos, J. 2011. A complete high resolution Paleocene benthic stable isotope record for the central Pacific (ODP Site 1209). *Paleoceanography* 26, PA2216. <https://doi.org/10.1029/2010PA002092>